

**NASA TECHNICAL  
MEMORANDUM**

NASA TM X-53974

**THE CHARACTERISTICS OF PENETRATION  
FOR A DOUBLE-SHEET STRUCTURE  
WITH HONEYCOMB**

By David W. Jex,  
Archie M. Miller, and  
Charles A. MacKay  
Space Sciences Laboratory

January 5, 1970

**CASE FILE  
COPY**

**NASA**

*George C. Marshall Space Flight Center  
Marshall Space Flight Center, Alabama*

1. REPORT NO. <b>TM X-53974</b>		2. GOVERNMENT ACCESSION NO.		3. RECIPIENT'S CATALOG NO.	
4. TITLE AND SUBTITLE <b>The Characteristics of Penetration for a Double-Sheet Structure With Honeycomb</b>				5. REPORT DATE <b>January 5, 1970</b>	
				6. PERFORMING ORGANIZATION CODE	
7. AUTHOR(S) <b>David W. Jex, Archie M. Miller, and Charles A. MacKay</b>				8. PERFORMING ORGANIZATION REPORT #	
9. PERFORMING ORGANIZATION NAME AND ADDRESS <b>George C. Marshall Space Flight Center Marshall Space Flight Center, Alabama 35812</b>				10. WORK UNIT NO.	
				11. CONTRACT OR GRANT NO.	
12. SPONSORING AGENCY NAME AND ADDRESS				13. TYPE OF REPORT & PERIOD COVERED <b>Technical Memorandum</b>	
				14. SPONSORING AGENCY CODE	
15. SUPPLEMENTARY NOTES <b>Prepared by Space Sciences Laboratory, Science and Engineering Directorate</b>					
16. ABSTRACT <p>The channeling of debris by a double-sheet structure separated by a honeycomb material has been reported by many investigators in the hypervelocity field. It has been suggested that this channeling will reduce the protective capability of such a structure when compared to an identical structure without honeycomb.</p> <p>A series of tests was conducted by this laboratory to gain an understanding of the characteristics of the channeling phenomena and the extent to which the channeling would affect the ballistic limit of a honeycombed structure.</p> <p>It was found that the particular honeycomb tested exhibited greater protective ability than an identical double-sheet structure without the honeycomb for velocities between 3.5 and 8.23 km/sec.</p> <p style="text-align: center;"><b>EDITOR'S NOTE</b></p> <p>Use of trade names or names of manufacturers in this report does not constitute an official endorsement of such products or manufacturers, either expressed or implied, by the National Aeronautics and Space Administration or any other agency of the United States Government.</p>					
17. KEY WORDS			18. DISTRIBUTION STATEMENT		
19. SECURITY CLASSIF. (of this report) <b>Unclassified</b>		20. SECURITY CLASSIF. (of this page) <b>Unclassified</b>		21. NO. OF PAGES <b>36</b>	22. PRICE <b>\$3.00</b>

## TABLE OF CONTENTS

	Page
SUMMARY .....	1
INTRODUCTION.....	2
EXPERIMENTAL PROCEDURE .....	2
Test Parameters .....	2
Test Results .....	3
CONCLUSIONS .....	7
APPENDIX A .....	9

## LIST OF ILLUSTRATIONS

Figure	Title	Page
1.	Location of failure area with respect to the initial impact point . . . . .	10
2.	Normal impacts . . . . .	11
3.	Honeycomb for normal impacts. . . . .	15
4.	Impacts at 45 degrees from the normal . . . . .	17
5.	Honeycomb of impacts at a 45-degree angle from the normal. . . . .	18
6.	Impacts at a 60-degree angle from the normal. . . . .	20
7.	Plot of the ballistic limit as a function of angle for honeycombed structure . . . . .	22
8.	Nonhoneycombed rear sheets . . . . .	23
9.	Nonhoneycombed rear sheets . . . . .	25

## LIST OF TABLES

Table	Title	Page
1.	Projectile Impacting Normal to Front Surface of the Target. . . . .	4
2.	Projectile Impacting at an Angle of 45 Degrees from the Normal to the Front Surface of the Target. . . . .	6
3.	Projectile Impacting at an Angle of 60 Degrees from the Normal to the Front Surface of the Target. . . . .	7



## THE CHARACTERISTICS OF PENETRATION FOR A DOUBLE-SHEET STRUCTURE WITH HONEYCOMB

### SUMMARY

The channeling of debris by a double-sheet structure separated by a honeycomb material has been reported by many investigators in the hyper-velocity field. The fact that the honeycombed structure will effectively channel or concentrate debris suggests that it will effectively reduce the protective capability of the structure when compared to an identical structure without honeycomb in which the debris is allowed to disperse over a large area.

A series of tests was conducted by this laboratory to gain an understanding of the characteristics of the channeling phenomena and the extent to which the channeling would affect the ballistic limit of a honeycombed structure. Two identical double-sheet structures were tested. One was separated by honeycomb, while the other was void between the sheets. These targets were examined in the velocity range of 3.5 km/sec to 8.23 km/sec.

The characteristic of failure for the honeycombed structures was a point concentration of small debris particles, resulting in a bulging and tearing failure of the rear surface of the target. This is the characteristic that prompts the suggestion that the protective capability will be reduced. The reasoning is that the momentum loading of several small debris particles concentrated at a point or finite area will fail at a lower input energy because several particles act on one point rather than being allowed to disperse and act on separate points. Contrary to this suggestion it was found that the honeycombed structure had a better protective capability than the same structure without honeycomb when the ballistic limits were compared.

The suggested explanation for this result lies in the sequence of events. The primary debris or fragments resulting from the initial impact undergo collisions with the honeycomb cell walls. This process generates smaller debris particles and channels them toward a point. The fragmentation and loss of energy associated with the secondary impacts overcompensates for the channeling effect, and the result is that the honeycombed structure has a better protective capability than the same structure without honeycomb.

At the velocities achieved in this test series, it is important to note that the target debris is in the solid fragment state. At velocities higher than those obtained in this test series, in which the liquid and gaseous states of the target debris are achieved, the channeling effect may dominate the failure. Consequently, the results may be exactly opposite as far as the protective capability is concerned.

## INTRODUCTION

The protection of personnel and instruments in space has motivated many studies to define the space environment. One of the hazards to which the personnel and instruments are subjected is the meteoroid environment. These small projectiles traveling at extremely high velocities can cause serious damage if sufficient protection is not afforded the spacecraft. It has been found that the most effective protection is given by a double-sheet structure in which the front sheet exposed to the meteoroid environment is thick enough to completely fragment the incoming meteoroid and spaced far enough in front of the second sheet to allow the debris to disperse.

In some applications of present spacecraft design it has been found advantageous to construct components in this double-sheet configuration with a honeycombed material between the sheets to add considerable strength with a minimum of added weight. In some applications this structure may be exposed to the meteoroid environment; therefore, the question arises as to the protective capability of such a structure. Many investigators have reported a noticeable channeling effect or concentration of debris exhibited by this configuration.

To determine the characteristics of this channeling phenomena and the extent to which it affects the ballistic limit of a given structure, a series of tests was conducted by this laboratory.

## EXPERIMENTAL PROCEDURE

### Test Parameters

Accelerators. The accelerator used for this test series was a two-stage, 1/16-in. light gas gun. Hydrogen was used to accelerate the projectile. The highest velocity obtained to date with this accelerator is 8.53 km/sec.

Range. The range has a free flight path approximately 6 m long. Along this free flight path are stationed three photomultiplier tubes and two photo FET transducers. The output signals of these five devices establish a time-of-flight from which the velocities are calculated.

The tests were conducted with a range pressure of 4 mm mercury created by introducing Argon into the range after evacuation. This environment was necessary to allow the photomultiplier tubes and photo FET transducers to establish time-of-flight.

Projectiles. The projectiles used for this test series were 1/16-in. cylinders with an l/d ratio equal to 1. The material used to make the cylinders was "Lexan," which has a density of 1.25 gm/cm<sup>3</sup>. The projectile mass was held constant at  $4.46 \pm 0.07$  mg.

Targets. There were two types of double-sheet targets used. They were made from identical material; however, one target had honeycomb between the front and rear sheet, while the other was void. The front and rear sheets of both targets were made of 7075-T6 aluminum. The front sheet thickness was 0.030 in. and the rear sheet thickness was 0.020 in. The total thickness of the targets was 0.95 in. The honeycomb had the following characteristics: 5052-H39 aluminum, MIL-C-7438; 0.001 in. thick; and 3/16-in. cells.

The choice of these target parameters was determined on the basis of the use of this particular honeycombed material in spacecraft.

## Test Results

The penetration threshold used for this test series is defined as a crack or hole through which light, originating from a back-lighting source, may be observed.

This test series examined three types of impacts on the honeycombed structure described: (1) normal impacts, (2) impacts at a 45-degree angle from the normal, and (3) impacts at a 60-degree angle from the normal.

In addition, nine impacts were conducted on an identical structure without honeycomb for comparison in determining the effect on the ballistic limit.

Honeycombed Structures. The failure area on the rear sheet, as related to the point of impact on the front sheet for the three cases examined, is illustrated in Figure 1. There are several characteristics in this figure that deserve special attention.

1. The failure area remains within the boundaries of the cell in which the initial impact occurred.

2. The failure area shifts from the center for normal impacts to the edge of the cell boundaries for impacts at a 60-degree angle from the normal.

3. The dashed lines, indicating damage to cell walls, illustrate that more damage occurs in the direction of the velocity vector.

Normal Impacts. The targets used on the 15 shots that contributed to the determination of the penetration threshold for normal impacts are illustrated in Figure 2. Photograph A is a typical view of the damage sustained by the front face of the honeycombed targets. Photographs B through P are rear surface views of the targets. Each view has the essential data and reference number illustrated. The resulting data are listed in Table 1.

TABLE 1. PROJECTILE IMPACTING NORMAL TO  
FRONT SURFACE OF THE TARGET

Velocity (km/sec)	Penetration (P); Not Penetrated (NP)	Firing Reference No.
8.32	P	D-1-001
7.39	P	D-1-002
6.79	P	D-1-011
6.78	P	D-1-005
6.64	P	D-1-003
6.52	P	D-1-014
6.25	P	D-1-007
5.60	P	D-1-008
5.42	P	D-1-010
5.17	P	D-1-016
4.65	P	D-1-018
4.44	P	D-1-017
4.22	NP	D-1-020
4.20	NP	D-1-012
4.10	NP	D-1-019

From examination of the failure areas it is evident that the characteristics of failure are: (1) a pressure pulse or momentum loading that bulged or stretched the material to the point of tearing, rather than a "punch-out" effect, and (2) as the penetration threshold is approached there is a noticeable point concentration of debris.

A view of the damage to the honeycomb itself is shown in Figure 3. Photographs A-1, B-1, and C-1 are views of the honeycomb if one is looking toward the front surface, when the structure is cut in the center. Photographs A-2, B-2, and C-2 are views of the honeycomb if one is looking toward the rear surfaces or failure areas when the structure is cut in the center. Photographs D and E are views of the honeycomb if one is looking toward the rear surface with the front surfaces removed. It is obvious from this that the radial damage to the honeycomb decreases as the velocity decreases. Although the radial damage to the honeycomb decreases with decreasing velocity, an examination of the failure on the rear surfaces of these targets in Figure 2 reveals that they are almost identical. There is an exception with D-1-001 #5, which is the target for the fastest velocity fired; the bulging and tearing failure is obvious. The exception is that the loading was great enough to dislodge a piece of the rear surface after the initial tearing failure was accomplished. Similar results are shown in other targets in the higher velocity region.

Examination of the inside surface of the rear sheets reveals that the loading that caused failure has characteristics of the erosive action of sand-blasting. Under magnification it appears pitted by small particles; however, the pitting did not cause the failure. The failure is characteristic of momentum loading of many small particles causing the material to bulge and tear.

The damage to the cell walls is of a different nature. There are various size holes, which are easily observed without magnification.

Impacts at 45 Degrees from the Normal. Five shots contributed to the determination of the penetration threshold for an impact at 45 degrees from the normal.

The data are listed in Table 2. See Figure 4 for a typical view of the front surface (photograph A) and for views of the rear surfaces (photographs B through F).

TABLE 2. PROJECTILE IMPACTING AT AN ANGLE OF 45 DEGREES FROM THE NORMAL TO THE FRONT SURFACE OF THE TARGET

Velocity (km/sec)	Penetration (P); Not Penetrated (NP)	Firing Reference No.
7.38	P	D-1-026
7.24	P	D-1-024
6.85	P	D-1-027
6.51	NP	D-1-023
6.48	NP	D-1-021

The point concentration of small particles is again obvious. The characteristic of bulging and tearing is again the cause of failure.

The photographs in Figure 5 are views of the honeycomb when one is looking toward the rear surfaces, and the front surfaces are removed. These photographs correspond to those in Figure 4. The radial honeycomb damage shows the same general decrease as the velocity decreases while the failure of the rear sheet remains identical, although the velocity range in this case is very limited. The damage to the cell walls was greater in the direction of the velocity vector and is even more apparent in the impacts at 60 degrees from the normal.

Impacts at 60 Degrees From the Normal. Only three shots were necessary to determine the penetration threshold at this angle. The data are listed in Table 3; Figure 6 shows a typical view of the front surface, damage to rear surfaces, and the honeycomb view (looking toward the rear surface) for each shot.

The failure area or point lies at the extreme boundary of the cell in which the initial impact occurred in the direction of the velocity vector as illustrated in Figure 1.

The damage to the cell walls in the direction of the velocity vector is very evident and pronounced in these three targets; however, when the inside surface of the rear sheet is examined, the only damaged area lies within the boundaries of the cell in which the initial impact occurred.

TABLE 3. PROJECTILE IMPACTING AT AN ANGLE OF 60 DEGREES FROM THE NORMAL TO THE FRONT SURFACE OF THE TARGET

Velocity (km/sec)	Penetration (P); Not Penetrated (NP)	Firing Reference No.
7.26	P	D-1-030
7.12	NP	D-1-028
7.05	NP	D-1-029
6.31	NP	D-1-031

The graph in Figure 7 plots the data obtained from this test series and shows the penetration threshold as a function of the angle.

The horizontal dashed line at 80 degrees indicates that within the velocity capabilities of this facility for the size projectile under study, there would be no penetration of the described structure above 80 degrees. This is based on a shot in which the projectile glanced off the front sheet without penetrating it.

Nonhoneycombed Structures. The nine impacts conducted on an identical structure without honeycomb ranged in velocity from 6.80 to below 4.00 km/sec. All impacts were normal to the front sheet. Figures 8 and 9 show the rear sheets of these targets. The failure in all cases was caused by individual fragments of debris. As the velocity drops, the sizes of the fragments increase, and the number of fragments decreases. Although there is an obvious change in the debris created by impact, the failure of the rear sheet remains almost identical. From the figures, it can be seen that for all impacts conducted, penetration of the second sheet was evidenced. This penetration is of the "punch-out" nature.

The ~ sign in Figures 8 and 9 indicates that the velocities expressed are not exact; however, they are within  $\pm 2$  percent.

## CONCLUSIONS

The suggestion that the protective capability of a double-sheet structure would be effectively reduced by the presence of honeycomb would seem to be supported by the point concentration or channeling evidenced by the honeycombed targets. However, when the ballistic limit of this honeycombed structure

(4.44 to 4.22 km/sec) is compared to the ballistic limit of the same structure without honeycomb (below 4 km/sec), it is evident that the honeycombed structure has a protective capability at least slightly superior to the same structure without honeycomb within the velocity range of 3.5 to 8.23 km/sec. The suggested explanation for this result lies in the sequence of events. The primary debris or fragments resulting from the initial impact undergo collisions with the honeycomb cell walls. This process generates smaller debris particles and channels them toward a point. The fragmentation and loss of energy associated with the secondary impacts overcompensates for the channeling effect, and the result is that the honeycombed structure has a better protective capability than the same structure without honeycomb.

At the velocities achieved in this test series, it is important to note that the target debris is in the solid fragment state. At velocities higher than those obtained in this test series, in which the liquid and gaseous states of the target debris are achieved, the channeling effect may dominate the failure. Consequently the results may be exactly opposite as far as the protective capability is concerned.



## APPENDIX A

A comparison was made to the following empirical formula derived by Robert Nysmith of Ames Research Center<sup>1</sup>.

$$B. L. = 3.34 \times 10^{-3} \left( \frac{t_1}{d} \right)^2 \left( \frac{t_2}{d} \right)^{3.75} \left( \frac{h}{d} \right)^5$$

where B. L. is the ballistic limit velocity in kilometers per second,  $t_1$  is the front sheet thickness,  $t_2$  is the rear sheet thickness,  $h$  is the spacing, and  $d$  is the diameter of the projectile. This formula was derived from a number of tests with Pyrex glass spheres impacting 2024-T3 aluminum double-sheet structures.

To make the comparison we calculated the diameter Pyrex sphere required to be equal in mass to the projectile we were using. The resulting substitutions yielded a ballistic limit of 6.85 km/sec.

The tests in Nysmith's publication were conducted with the front plate being thinner than the rear plate in all cases. In the structure under test this was not true. However, a series of three shots on the structure without honeycomb rearranged so that the thinner of the two sheets became the front sheet yielded a ballistic limit between 6.85 and 7.08 km/sec.

- 
1. C. Robert Nysmith, Compilation of Papers from the OART Meteoroid Impact and Penetration Workshop, Manned Spacecraft Center, October 1968, pp. 412-418.

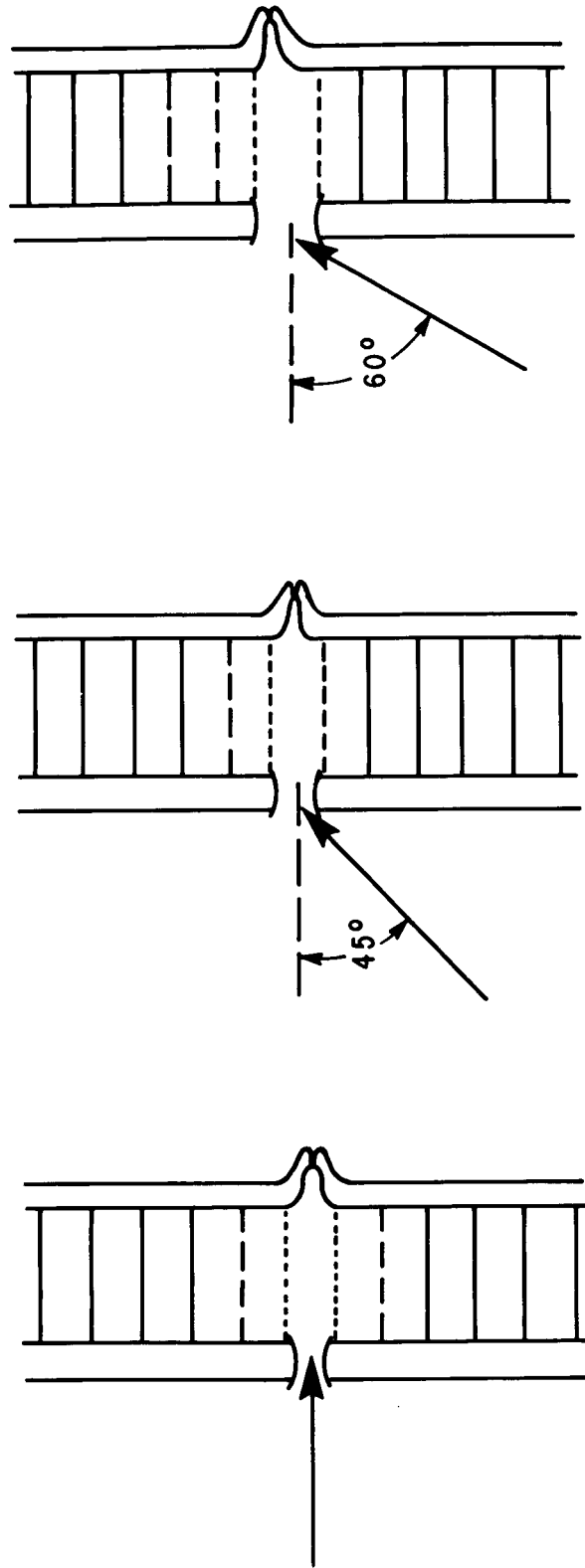
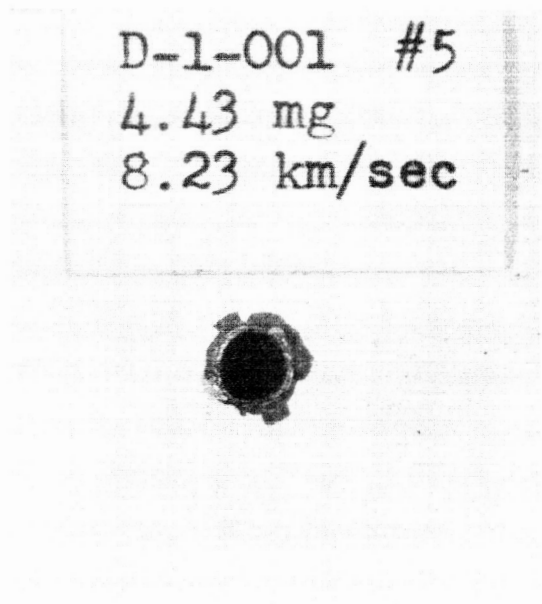
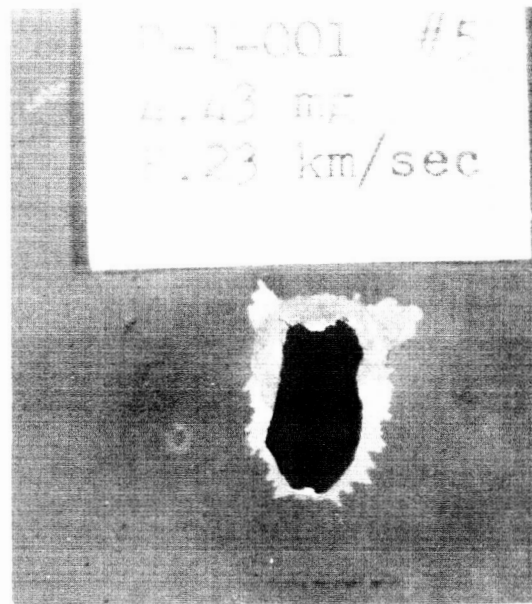


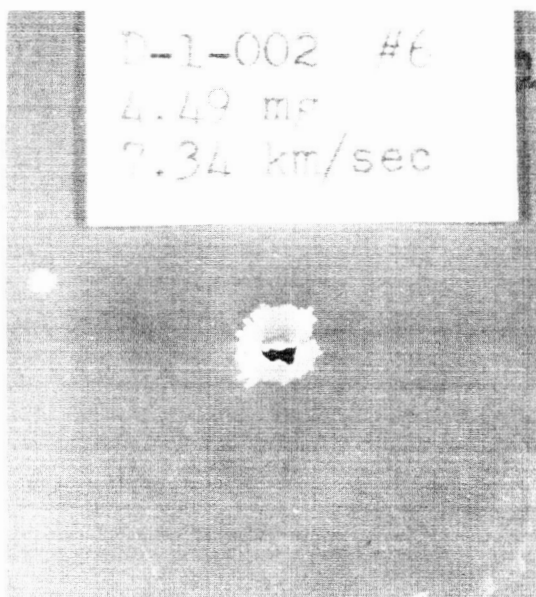
Figure 1. Location of failure area with respect to the initial impact point.



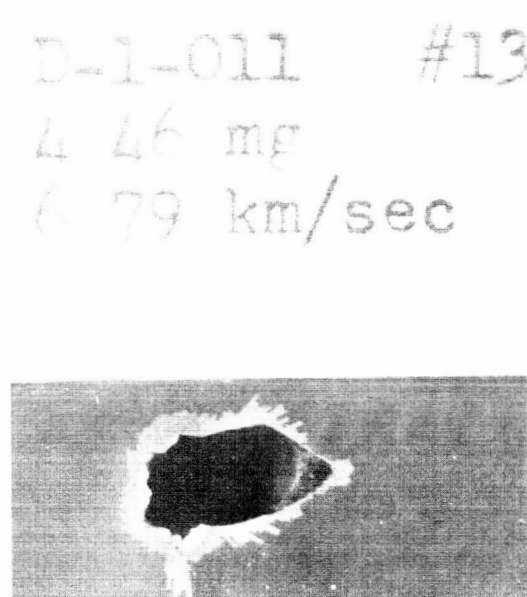
A



B

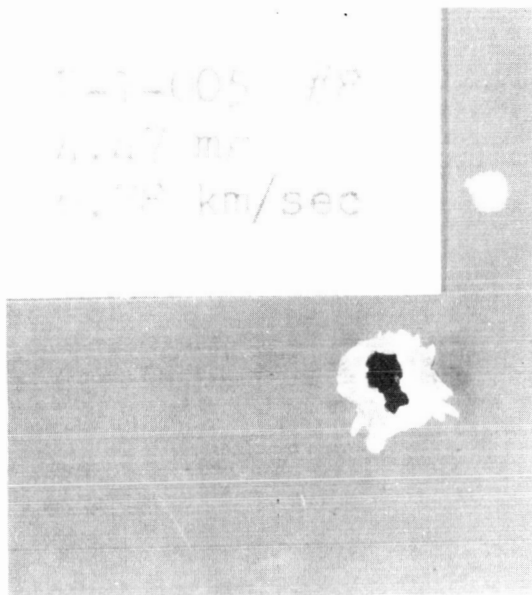


C

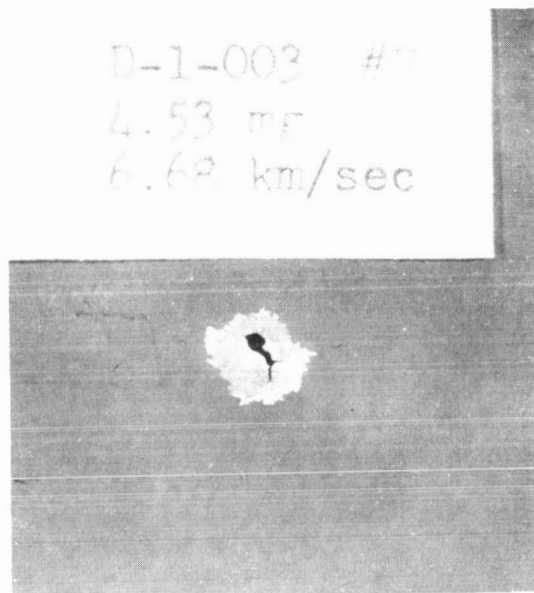


D

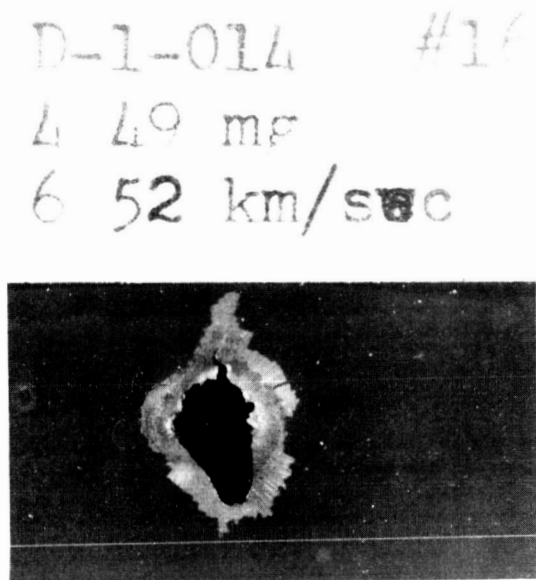
Figure 2. Normal impacts.



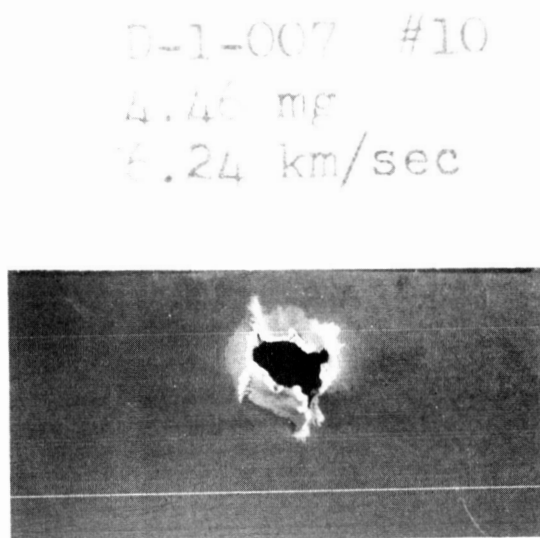
E



F



G



H

Figure 2. (Continued).

D-1-008 #11  
4.43 mg  
5.62 km/sec



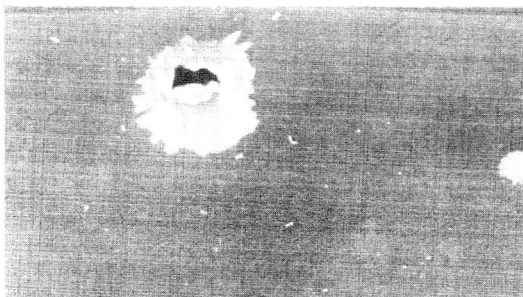
I

D-1-010 #12  
4.44 mg  
5.47 km/sec



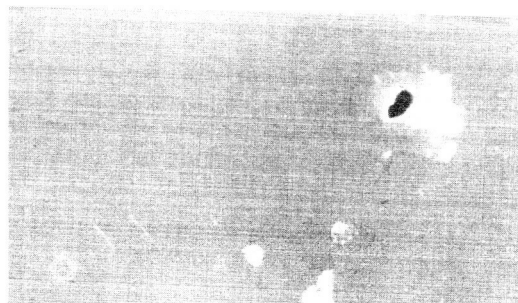
J

D-1-016 #6  
4.49 mg  
5.17 km/sec



K

D-1-017 #31  
4.44 mg  
5.17 km/sec



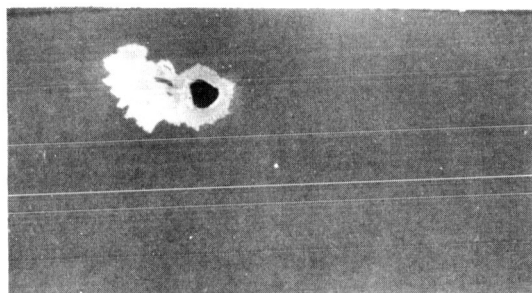
L

Figure 2. (Continued).

D-1-017 #4

4.46 mf

4.44 km/sec

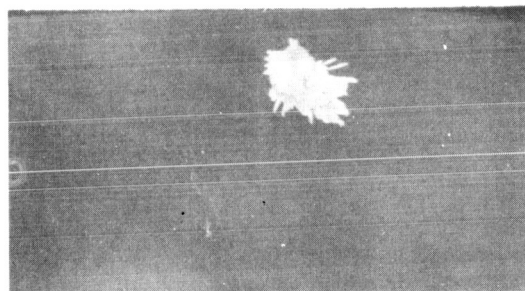


M

D-1-020 #8

4.48 mf

4.22 km/sec

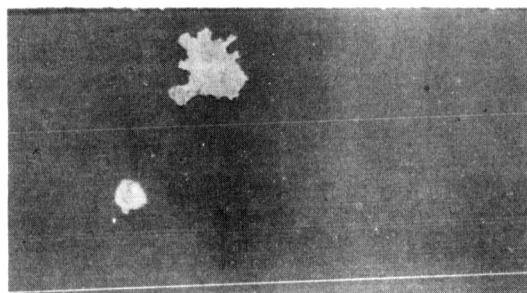


N

D-1-012 #14

4.49 mf

4.20 km/sec

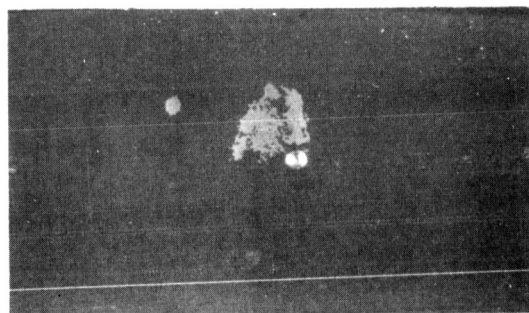


N

D-1-010 #10

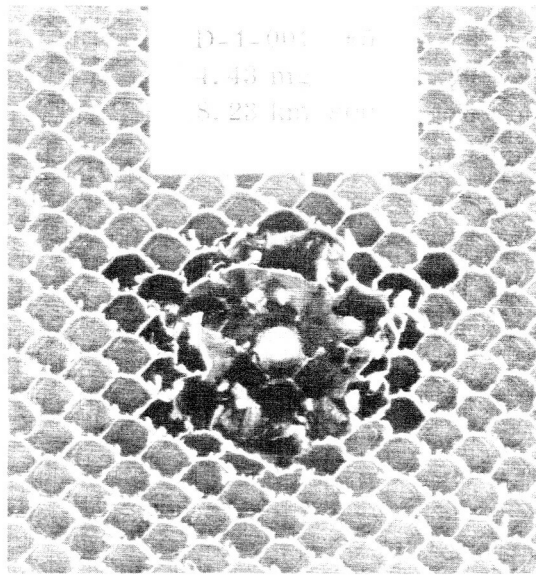
4.48 mf

4.10 km/sec

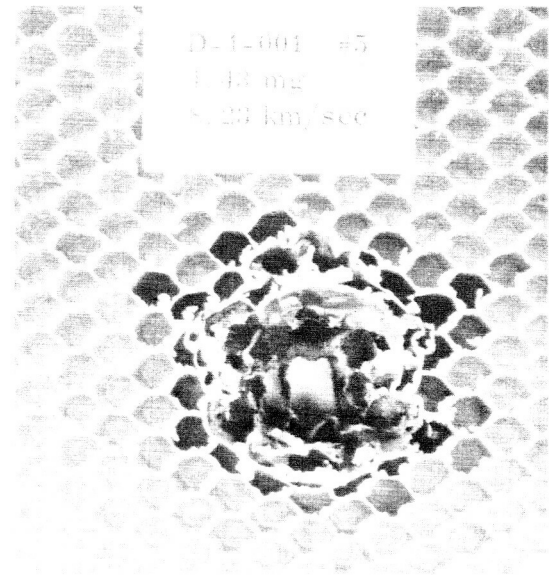


O

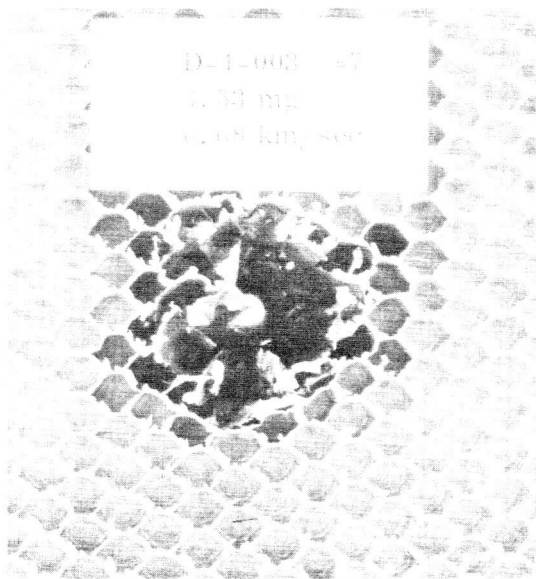
Figure 2. (Concluded).



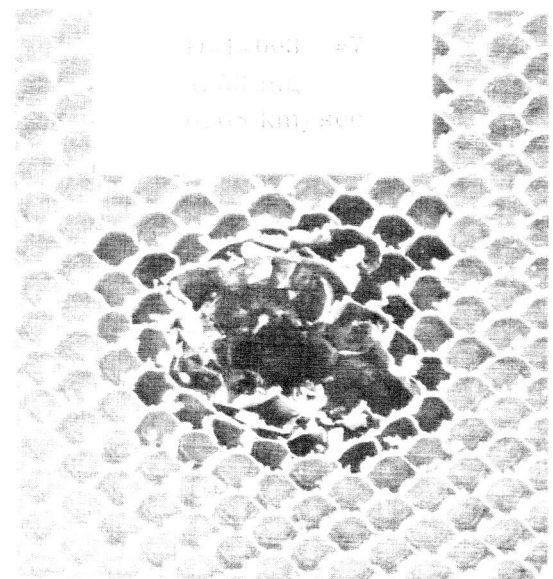
A-1



A-2

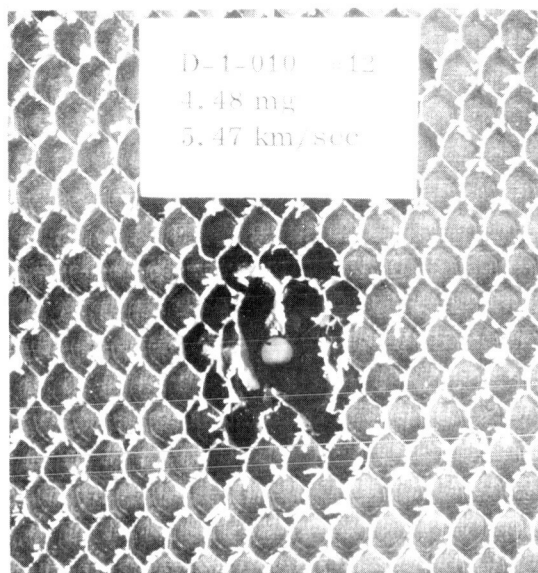


B-1

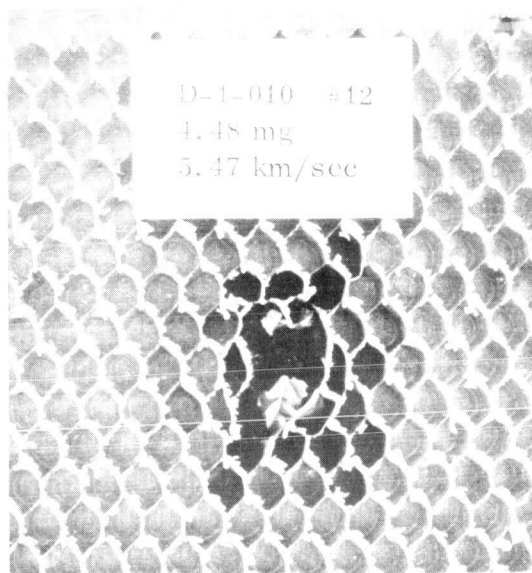


B-2

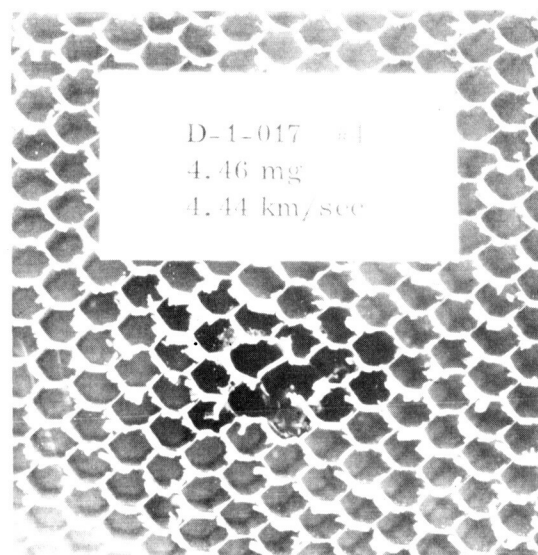
Figure 3. Honeycomb for normal impacts.



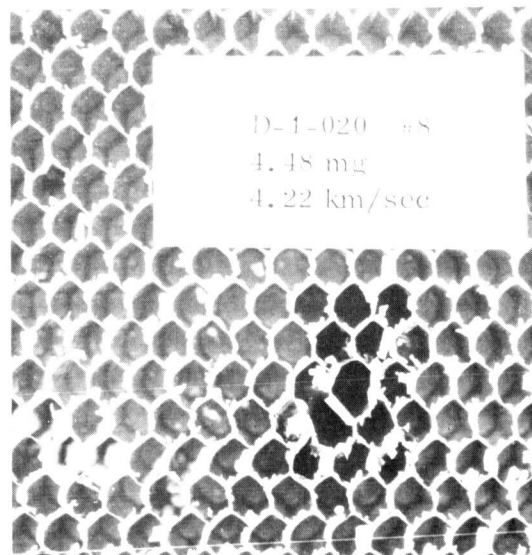
C-1



C-2



D

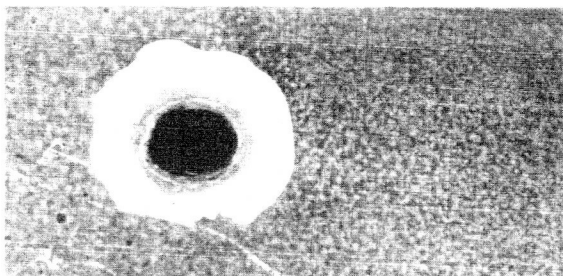


E

Figure 3. (Concluded).

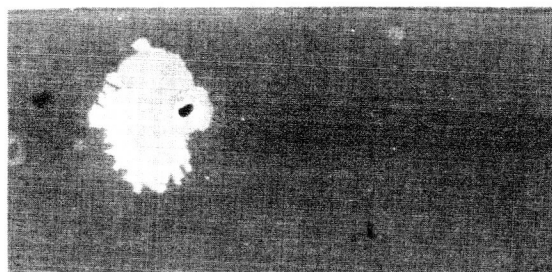


D-1-021 #1  
4.40 mg (45°)  
6.48 km/sec



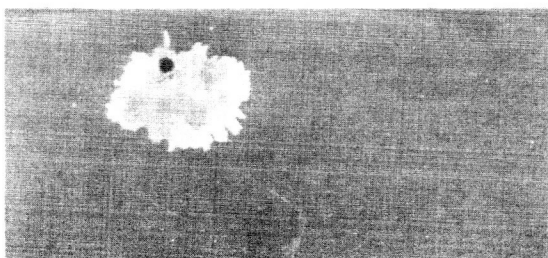
A

D-1-026 #15  
4.48 mg (45°)  
7.38 km/sec



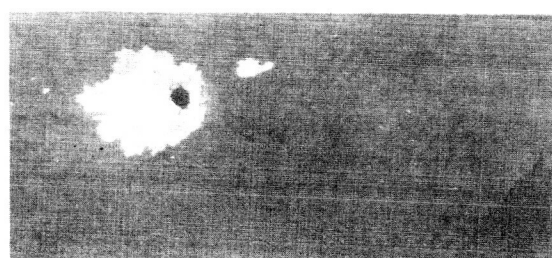
B

D-1-024 #15  
4.42 mg (45°)  
7.24 km/sec



C

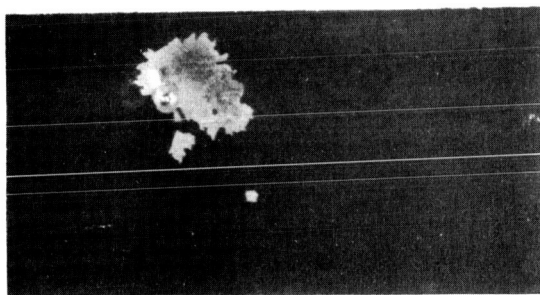
D-1-027 #1  
4.53 mg (45°)  
6.85 km/sec



D

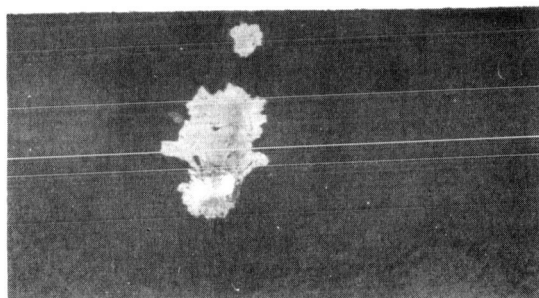
Figure 4. Impacts at 45 degrees from the normal.

D-1-023 #1  
 4.49 mg (45°)  
 6.51 km/sec



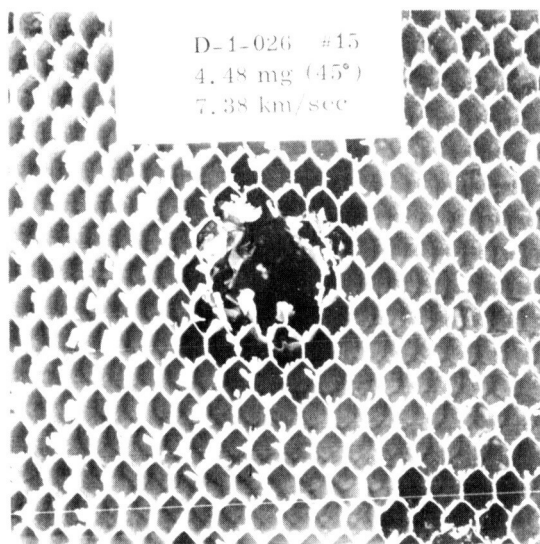
E

D-1-021 #1/  
 4.40 mg (45°)  
 6.48 km/sec



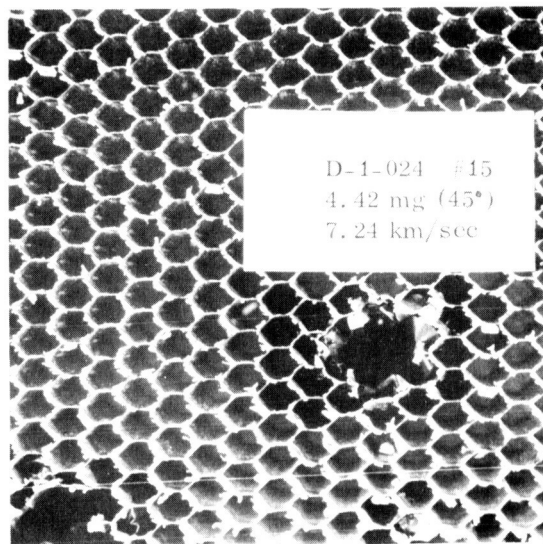
F

Figure 4. (Concluded).



D-1-026 #15  
 4.48 mg (45°)  
 7.38 km/sec

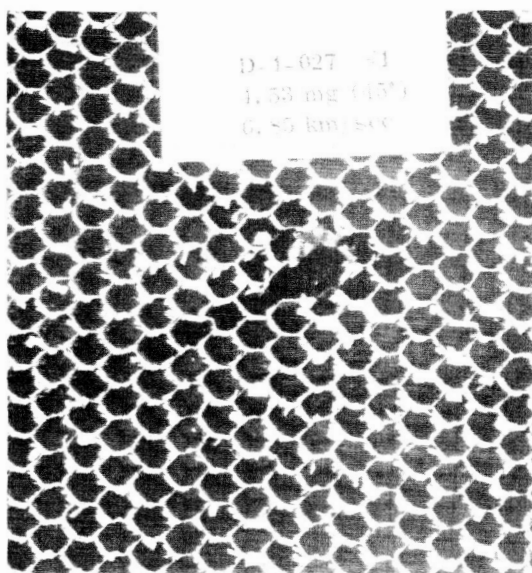
A



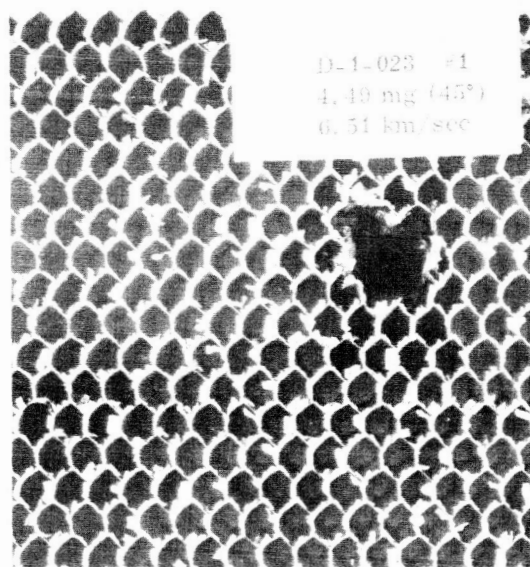
D-1-024 #15  
 4.42 mg (45°)  
 7.24 km/sec

B

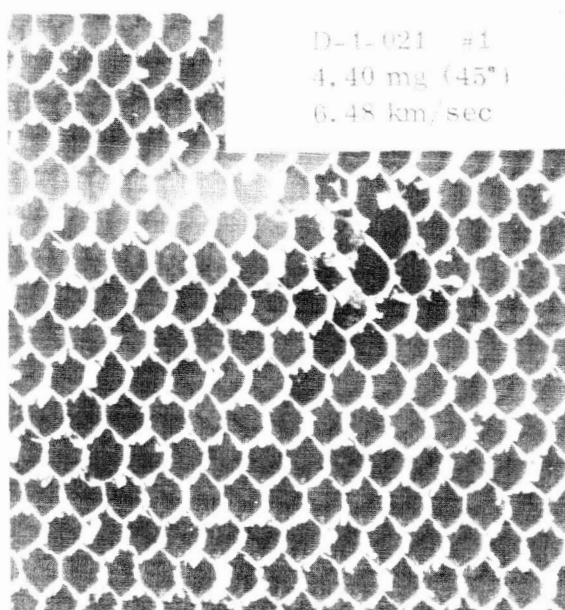
Figure 5. Honeycomb of impacts at a 45-degree angle from the normal.



C



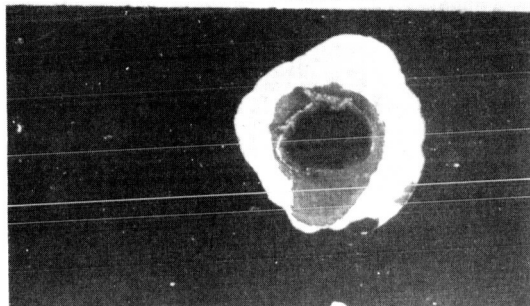
D



E

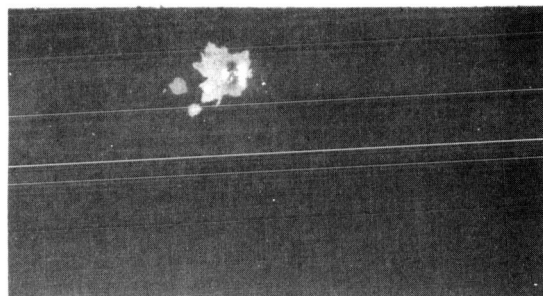
Figure 5. (Concluded).

D-1-028 #3  
4.43 mg (60°)  
7.12 km/sec



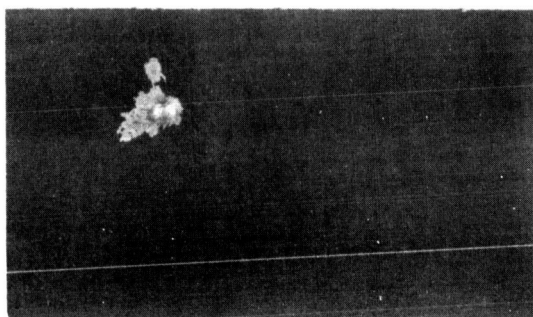
A

D-1-030 #3  
4.49 mg (60°)  
7.26 km/sec



B

D-1-028 #3  
4.43 mg (60°)  
7.12 km/sec



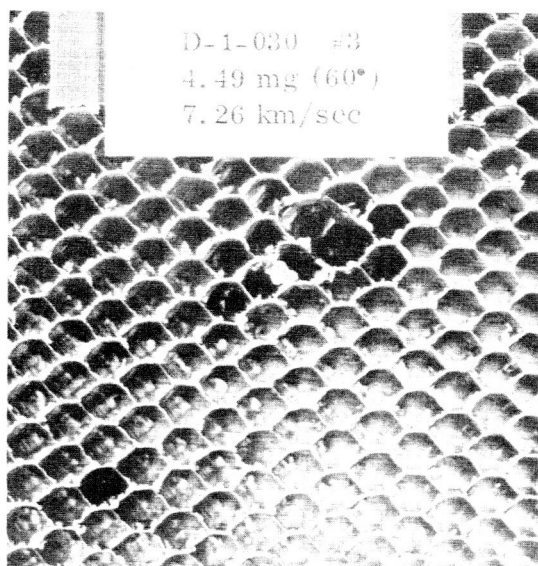
C

D-1-029 #3  
4.49 mg (60°)  
7.05 km/sec

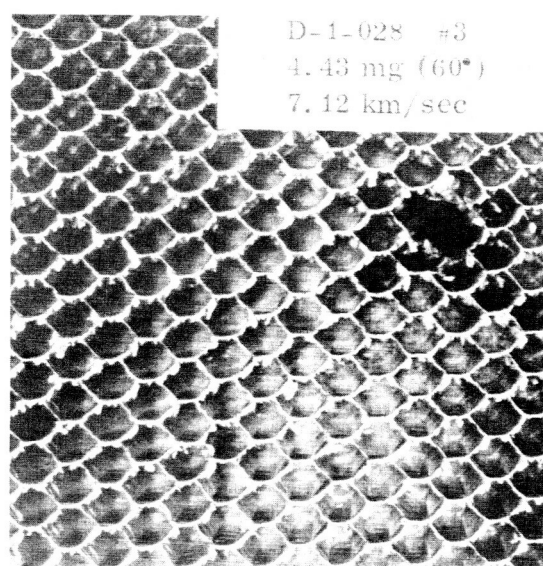


D

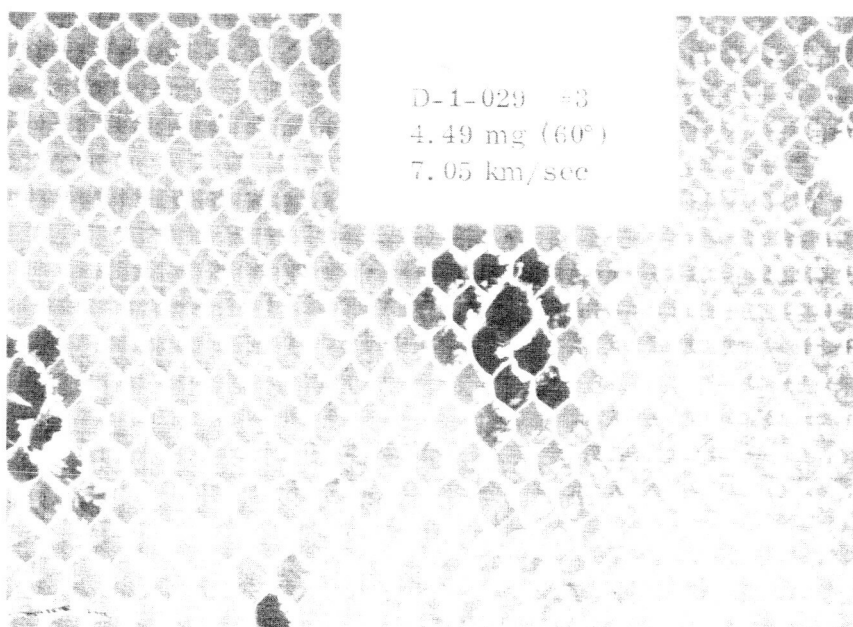
Figure 6. Impact at a 60-degree angle from the normal.



E



F



G

Figure 6. (Concluded).

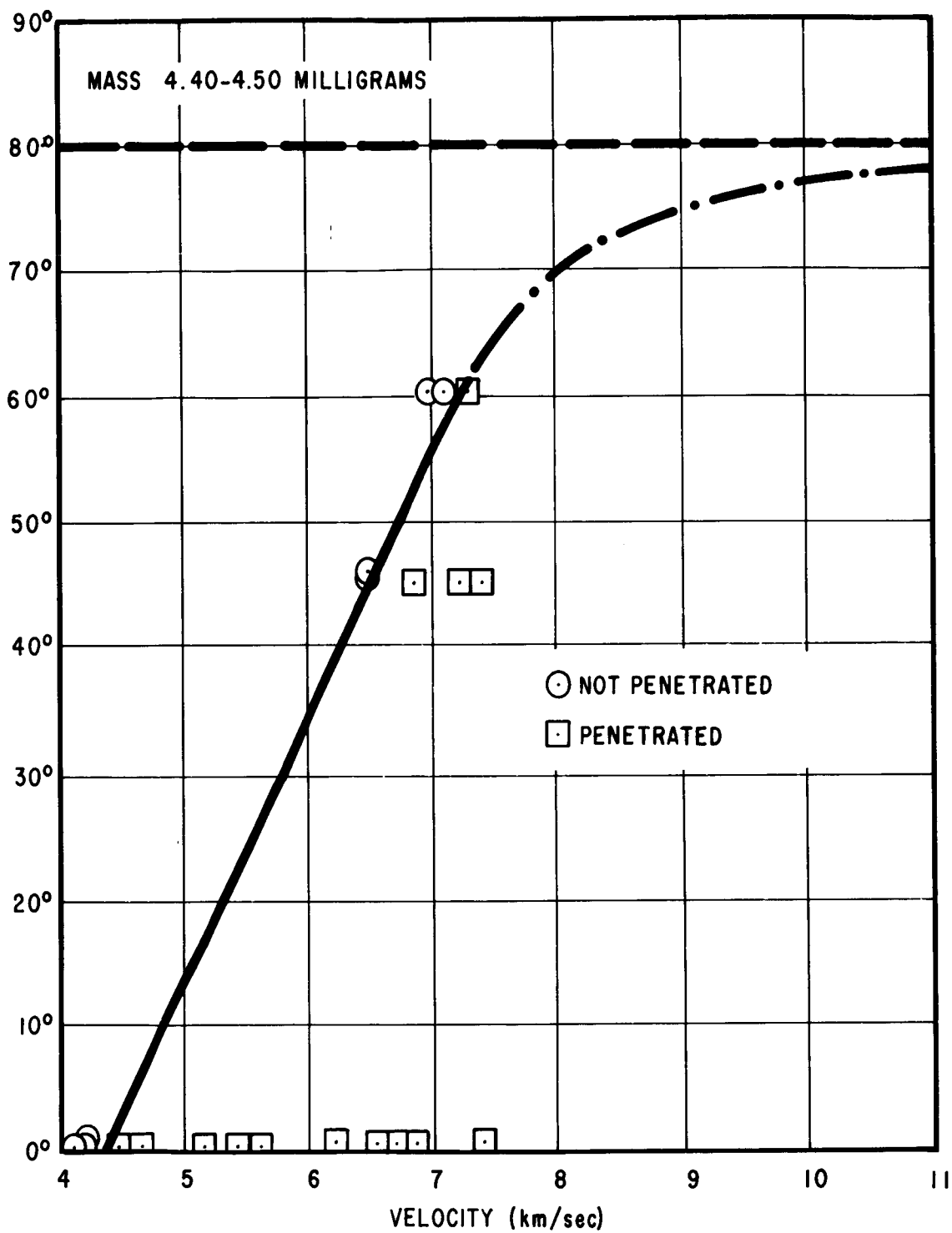
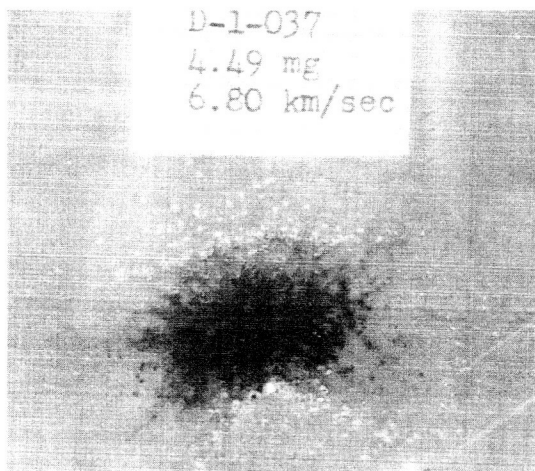
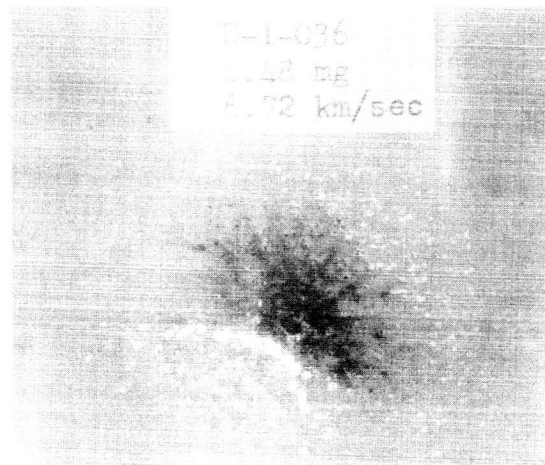


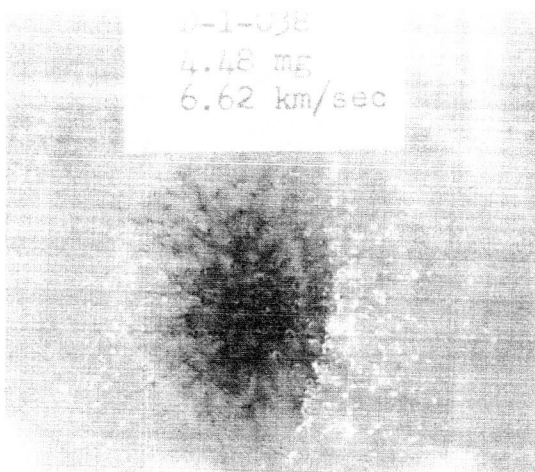
Figure 7. Plot of the ballistic limit as a function of angle for honeycombed structure.



A



B



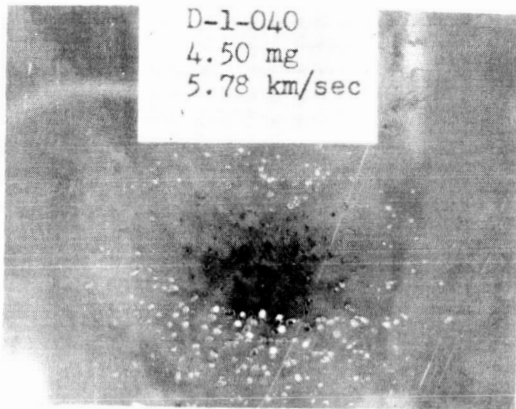
C



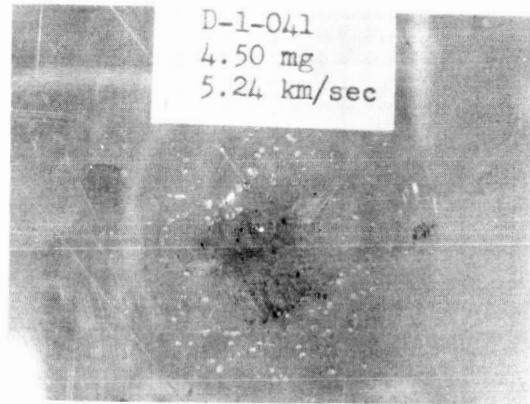
D

Figure 8. Nonhoneycombed rear sheets (front surface).

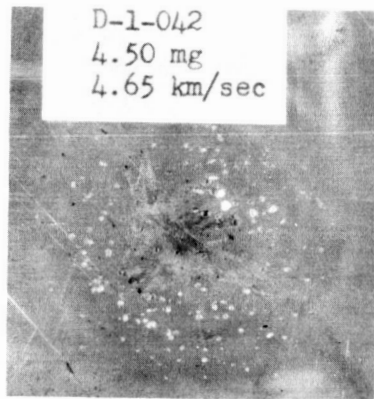




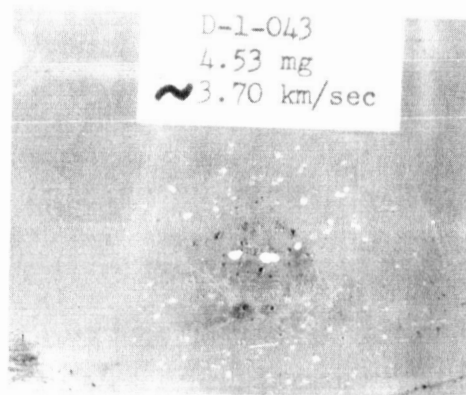
E



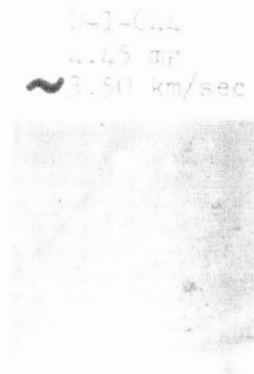
F



G



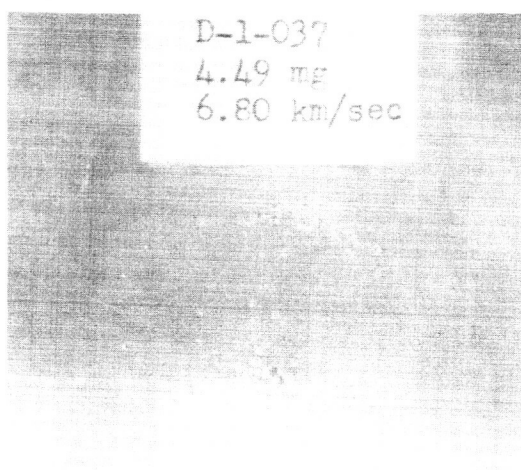
H



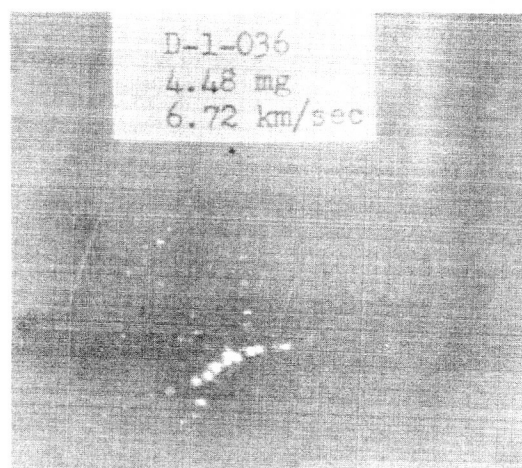
I

Figure 8. (Concluded).

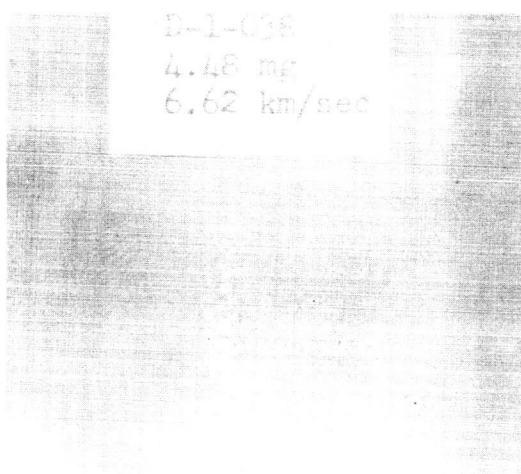




A



B

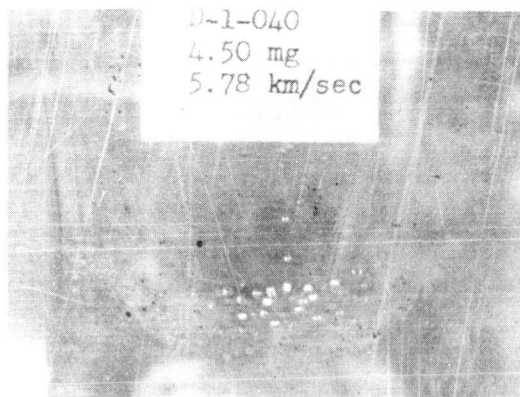


C



D

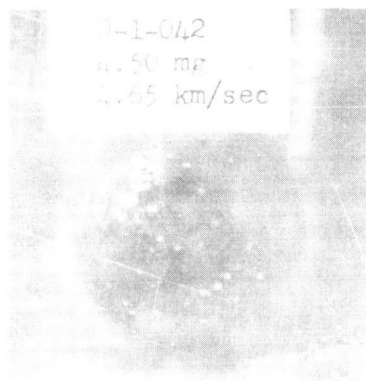
Figure 9. Nonhoneycombed rear sheets (rear surface).



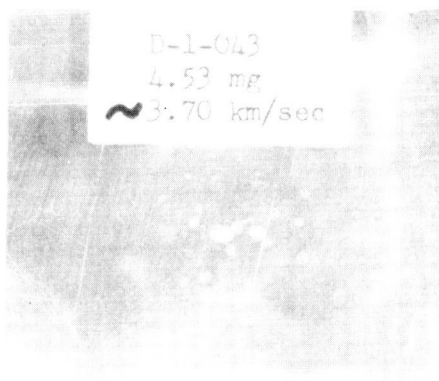
E



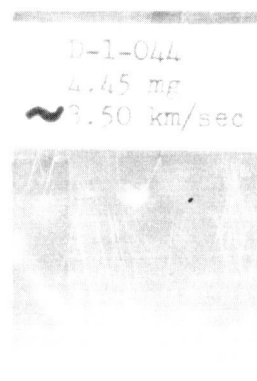
F



G



H



I

Figure 9. (Concluded).

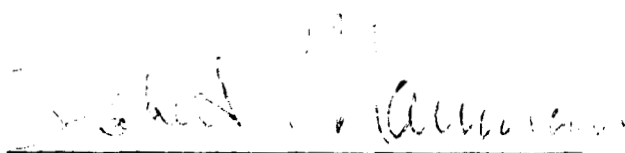
## APPROVAL

# THE CHARACTERISTICS OF PENETRATION FOR A DOUBLE-SHEET STRUCTURE WITH HONEYCOMB

By David W. Jex, Archie M. Miller, and Charles A. MacKay

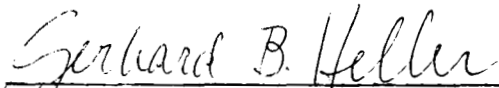
The information in this report has been reviewed for security classification. Review of any information concerning Department of Defense or Atomic Energy Commission programs has been made by the MSFC Security Classification Officer. This report, in its entirety, has been determined to be unclassified.

This document has also been reviewed and approved for technical accuracy.



---

ROBERT J. NAUMANN  
Chief, Physics and Astrophysics Division



---

GERHARD B. HELLER  
Director, Space Sciences Laboratory

# DISTRIBUTION

TM X-53974

## INTERNAL

### DIR

Dr. von Braun  
Mr. Foster

### DEP-T

Dr. Rees

### DEP-A&TS

Mr. Newby

### AD-S

Dr. Stuhlinger

### S&E-DIR

Mr. Weidner  
Mr. Cook

### S&E-AERO-DIR

Dr. Geissler

### A&E-AERO-T

Mr. Murphree  
Mr. Lavender

### S&E-AERO-Y

Mr. Vaughan  
Mr. Dalton  
Mr. Smith

### S&E-ASTR-DIR

Mr. B. Moore

### S&E-ASTR-IRT

### S&E-ASTR-M

### S&E-R-DIR

Dr. Johnson  
Miss Smith

### A&E-ME-DIR

Dr. Seibel

### S&E-ASTN-DIR

Mr. Heimburg

### S&E-SSL-DIR

Mr. Heller

### S&E-SSL-X

Dr. Decher  
Dr. Weber

### S &E-SSL-C

Mr. Mathis  
Reserve (20)

### S&E-SSL-P

Mr. Naumann  
Dr. Dozier  
Mr. Chisholm

### S&E-SSL-PM

Mr. Espy  
Mr. Clifton  
Mr. Jex (10)

### S&E-SSL-PA

Mr. Holland

### S&E-SSL-N

Mr. Stern

### S&E-SSL-T

Mr. Snoddy  
Mr. Jones

## DISTRIBUTION (Continued)

### INTERNAL (Concluded)

S&E-SSL-S

Dr. Seiber

PA

Mr. Slattery

A&TS-PAT

Mr. Wofford

A&TS-MS-H

A&TS-MS-IP (2)

A&TS-MS-IL (8)

A&TS-TU (6)

PM-PR-M

### EXTERNAL

National Aeronautics and Space  
Administration  
Washington, D. C. 20546:

Dr. George E. Mueller, M  
Maj. Gen. Samuel C. Phillips, MA  
Dr. Homer E. Newell, A  
Dr. Maurice Dubin, SG  
Mr. Jesse L. Mitchell, SG  
Dr. Henry J. Smith, SG  
Dr. Nancy G. Roman, SG  
Mr. Bruce Lundin, R  
Dr. Raymond H. Wilson, Jr., RRA  
Mr. Milton B. Ames, Jr., RV  
Mr. E. O. Pearson, RV-1  
Mr. J. W. Keller, RV-1  
Mr. C. T. D'Aiutolo, RV-1

Scientific and Technical Information

Facility (25)

Attn: NASA Representative (S-AK/RKT)

P. O. Box 33

College Park, Maryland 20740

Darrell E. Munson

5163

Sandia Corporation

Albuquerque, New Mexico 87115

Robert Ratay

Structural Mechanics Section

Plt. 35, Dept. 462

Grumman Aircraft Corporation

Bethpage, New York

Basil Leftheris

Research Section

Plt. 35, Dept 582

Grumman Aircraft Corporation

Bethpage, New York

S. Shields

LTV Aerospace

Missile and Space Division

Unit 3-52100

Grand Prairie, Texas

Verne C. Frost

Aerospace Corporation

Solid Mechanics Department

Applied Mechanics Division

2350 East El Segundo Boulevard

El Segundo, California

## DISTRIBUTION (Continued)

### EXTERNAL (Continued)

Prof. William Golberg  
AFIT — SEB  
Wright-Patterson AFB, Ohio 45433

R. K. Watanabe  
The Boeing Company  
P.O. Box 3999  
Mail Stop 8H37  
Seattle, Washington

C. Robert Nysmith  
Ames Research Center  
Moffett Field, California

Dr. Benoit Jean  
Computing Devices of Canada  
Bell Corners  
Ottawa, Ontario, Canada

Burton G. Cour-Palais  
NASA — Manned Spacecraft Center  
Houston, Texas

Tom Lee  
NASA — Manned Spacecraft Center  
Houston, Texas

Walt Turner  
Brown Engineering Co.  
Mail Stop 132  
Huntsville, Ala. 35807

ARO, Inc.  
von Karman Gas Dynamics Facility  
Arnold Engineering Development Center  
Arnold Air Force Station, Tennessee  
37389  
Attn: Jack D. Whitfield

Avco Corporation  
Research and Advanced Development Division  
201 Lowell Street  
Wilmington, Massachusetts 01887  
Attn: W. Reinecke

Ballistics Research Laboratories  
Aberdeen Proving Ground,  
Maryland 21005  
Attn: AMXBR-EB, W. Braun

Canadian Armament Research and  
Development Establishment  
P. O. Box 1427  
Quebec 2, P. Q., Canada  
Attn: A. Lemay

Computing Devices of Canada, Ltd.  
Space Sciences Laboratory  
P. O. Box 508  
Ottawa 4, Ontario, Canada  
Attn: J. R. Murphy

Douglas Aircraft Company, Inc.  
3000 Ocean Park Blvd., Loc. A-10  
Santa Monica, California 90406  
Attn: R. N. Teng

Denver Research Institute  
University Park  
Denver, Colorado 80210

General Motors Corporation  
AC Electronics  
Defense Research Laboratories  
6767 Hollister Ave.,  
Goleta, California 93017  
Attn: W. K. Rogers

## DISTRIBUTION (Concluded)

### EXTERNAL (Concluded)

General Motors Corporation  
Manufacturing Development  
G. M. Technical Center  
12 Mile and Mound Road  
Warren, Michigan 48090  
Attn: A. R. McMillan

IIT Research Institute  
10 W. 35th Street  
Chicago, Illinois 60616  
Attn: M. S. Nusbaum

Institut Franco-Allemand de Recherches  
de Saint-Louis  
12, rue de l'Industrie  
Saint-Louis (Haut-Rhin)  
France  
Attn: C. L. Lecomte

Monsieur le Directeur du L. R. B. A  
Laboratoire de Recherches Balistiques  
et Aerodynamiques  
Vernon (Eure)  
France

Lincoln Laboratory  
Massachusetts Institute of Technology  
Lexington, Massachusetts 02173  
Attn: Dr. R. E. Slattery

Ames Research Center, NASA  
Moffett Field, California 94035  
Attn: Robert J. Carros Mail Stop 237-1

U. S. Naval Ordnance Laboratory  
White Oak, Silver Spring  
Maryland 20910  
Attn: J. N. Fedenia Code 321

U. S. Naval Research Laboratory  
Washington D. C. 20390  
Attn: J. R. Baker Code 5186

Royal Armament Research and  
Development Establishment  
Fort Halstead  
Sevenoaks, Kent  
England  
Attn: F. Smith, S/D4

University of Dayton Research  
Institute  
University of Dayton  
Dayton, Ohio 45409  
Attn: H. F. Swift